5 Experiments

5.1 FEM solver

In the following three subsections we will investigate the liability of our finite element solver on the variational problem; find $(u, \hat{u}) \in H^1(\Omega) \times H^1(\Gamma)$ such that

$$B[(u, \hat{u}), (v, \hat{v})]) = l[(v, \hat{v})] \qquad \forall (v, \hat{v}) \in H^1(\Omega) \times H^1(\Gamma) \tag{21}$$

where

$$B[(u, \hat{u}), (v, \hat{v})]) = \int_\Omega \nabla u \cdot \nabla v + \int_\Gamma \nabla \hat{u} \cdot \nabla \hat{v} + \int_\Gamma \gamma (u - \hat{u})(v - \hat{v}). \tag{22}$$

To study our solver we will use the method of manufactured solutions, hence we let

$$l[(v, \hat{v})] = \int_\Omega fv + \int_\Gamma \hat{f}\hat{v} - gv$$

to be able to enforce the manufactured solution as the solution to (21) - this will be described in more detail in 5.1.1. Convergence of the computed solution $(u_h, \hat{u}_h)$ to our manufactured solution $(u_m, \hat{u}_m)$ is our main concern and will be shown for different curves Γ - allowing for manufactures solutions with different properties. The convergence rates is then compared to known a priori estimates.

To discretize our domain we use Gmsh [Geuzaine and Remacle, 2009] and our solver is implemented using Gridap [Badia and Verdugo, 2020]. We use both first and second order interpolating polynomials, and quadrilateral and triangle elements to discretize our domain. We follow the notation used in [Elman et al., 2014], where P represents triangle elements, Q represents quadrilateral elements and k is the order of the interpolating polynomials.

5.1.1 Manufactured solutions on straight line domain and basic estimates

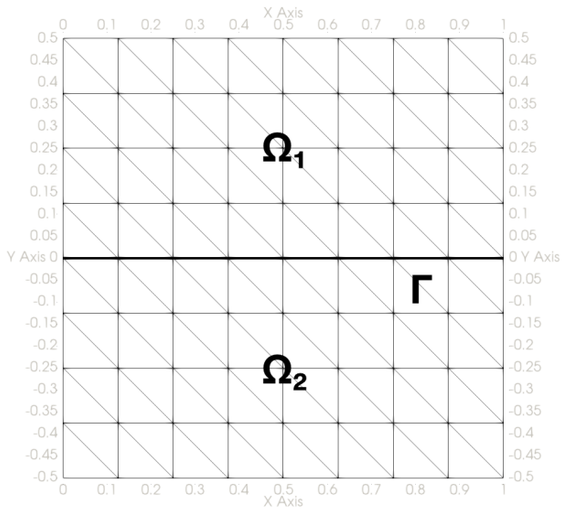

Figure 2: Square mesh with straight line embedded interface.

We define Ω as the square with verticies $(0, 0.5), (1, 0.5), (1, -0.5)$ and $(0, -0.5)$ and the subdomains $\Omega_1 = \{(x, y) \in \Omega | y > 0\}$ and $\Omega_2 = \{(x, y) \in \Omega | y < 0\}$. The one dimensional curve is embedded in Ω as $\Gamma = \{(x, y) \in \Omega | y = 0\}$. The corresponding strong formulation of (21) is then

$$\begin{aligned} -\Delta u_1 &= f_1 \qquad \text{on} \quad \Omega_1 \\ -\Delta u_2 &= f_2 \qquad \text{on} \quad \Omega_2 \\ u_1 = u_2 &= u_m \qquad \text{on} \quad \partial\Omega \setminus \Gamma \end{aligned} \tag{23}$$

$$\text{on } \Gamma \quad \begin{cases} -\Delta \hat{u} + \gamma(\hat{u} - u) & = \hat{f} \\ \hat{u}|_{\partial\Gamma} & = \hat{u}_m \\ u_1 - u_2 & = 0 \\ -\nabla u_1 \cdot \nu_1 - \nabla u_2 \cdot \nu_2 & = \gamma(u - \hat{u}) + g \end{cases} . \tag{24}$$

To see the relation (23), (24) $\rightarrow$ (21) we follow the standard procedure of multiplying with test functions and integrating over the domain, we define $v_1 = v|_{\Omega_1}$, $v_2 = v|_{\Omega_2}$, $u_1 = u|_{\Omega_1}$, $u_2 = u|_{\Omega_2}$ and require continuity; $v_1 - v_2 = u_1 - u_2 = 0$ on Γ. Using integration by parts and Green's identity we get

$$\left.\begin{aligned}\int_{\Omega_1} \nabla u_1 \cdot \nabla v_1 &= \int_{\Omega_1} f_1 v_1 + \int_{\partial\Omega_1} (\nabla u_1 \cdot \nu_1) v_1 \\ \int_{\Omega_2} \nabla u_2 \cdot \nabla v_2 &= \int_{\Omega_2} f_2 v_2 + \int_{\partial\Omega_2} (\nabla u_2 \cdot \nu_2) v_2\end{aligned}\right\} \rightarrow \int_\Omega \nabla u \cdot \nabla v = \int_\Omega fv - \int_\Gamma (\nabla u_1 \cdot \nu_1 + \nabla u_2 \cdot \nu_2) v$$
$$= \int_\Omega fv + \int_\Gamma \gamma(u - \hat{u})v + gv \tag{25}$$

where we have inserted g from (24) and set $v = 0$ on $\partial\Omega \setminus \Gamma$ such that the boundary term vanishes on $\partial\Omega \setminus \Gamma$ and the remainder is a Neumann term over Γ. Similarly, we get

$$\int_\Gamma \nabla\hat{u} \cdot \nabla\hat{v} + \gamma(\hat{u} - u)\hat{v} = \int_\Gamma \hat{f}\hat{v}. \tag{26}$$

Note that since Γ is one dimensional, there does not appear a Neumann term and for the gradient in Γ we have $\nabla = \frac{d}{dx}$, we do however keep the notation ∇ for consistency. Combining (25) and (26) we obtain the variational formulation; Find $(u, \hat{u}) \in H^1_D(\Omega) \times H^1_D(\Gamma)$ s.t.

$$\int_\Omega \nabla u \cdot \nabla v + \int_\Gamma \nabla\hat{u} \cdot \nabla\hat{v} + \int_\Gamma \gamma(u - \hat{u})(v - \hat{v}) = \int_\Omega fv + \int_\Gamma \hat{f}\hat{v} - gv$$
$$\forall (v, \hat{v}) \in H^1_0(\Omega) \times H^1_0(\Gamma) \tag{27}$$

where the $H^1_D(X) = \{u \in H^1(X) | u = g_D \text{ on } \partial X\}$ where g_D is some Dirichlet boundary condition, in this case we simply set $g_D = u_m$, and $H^1_0(X) = \{u \in H^1(X) | u = 0 \text{ on } \partial X\}$.

Using equation (23) and (24) we can construct manufactured solutions by choosing $u_m = u$, $\hat{u}_m = \hat{u}$ and calculating the corresponding $f, \hat{f}$ and g. With these source terms, our solutions $(u_h, \hat{u}_h)$ to (27) should approximate our manufactured solutions $(u_m, \hat{u}_m)$.

In our basic estimates we want to control that our solver [Badia and Verdugo, 2020] can approximate our manufactured solutions exactly when the order of our interpolating polynomials and the manufactured solutions agree. We also show that the solver behaves as expected for no coupling ($\gamma = 0$) and weak coupling ($\gamma = 1$). The error is measured with the H^1 norm

$$e_{tot} := \sqrt{\|u - u_h\|^2_{H^1(\Omega)} + \|\hat{u} - \hat{u}_h\|^2_{H^1(\Gamma)}}.$$

	γ = 0		γ = 1	
Manufactured Solutions	H^1-error	e_{tot}	H^1-error	e_{tot}
$u_m = x - y$	2.9e-15	2.9e-15	2.2e-15	3.5e-15
$\hat{u}_m = x$	4.1e-15		2.7e-16	
$u_m = x - y$	2.9e-15	0.072	7.3e-4	0.072
$\hat{u}_m = x^2$	0.072		0.072	
$u = \cos(x)_m + \sin(y)$	0.032	0.037	0.032	0.037
$\hat{u} = \sin(x)$	0.019	0.019		

Table 1: Manufactured solutions for (27). Script: m1.jl, mesh: mesh_1.msh

Table 1. shows the error for different manufactured solutions. We have used $P1$ elements in our approximations and should therefore expect machine precision for manufactured solutions of polynomial degree $k = 1$. The table shows that this is the case and we also note that the approximation error inflicts on u when the coupling factor $\gamma \neq 0$ and $\hat{u}$ is a higher order polynomial, even though u is a first order polynomial.

We recall our estimate

$$\|u-u_h\|_{H^1}^2+\|\hat{u}-\hat{u_h}\|_{H^1}^2 \leq (1+\gamma)^2\left[C(\Omega)h_\Omega^2\|D^2u\|_{L^2(\Omega)}^2+C(\Gamma)h_\Gamma^2\|D^2\hat{u}\|_{L^2(\Gamma)}^2\right]$$

and note that since the line segments in the discretion of the 1D domain Γ is also the edges of the neighboring elements in the discretion of the 2D domain Ω we have $h_\Gamma \leq h_\Omega$, therefore, we let $h = h_\Omega$ and get

$$\|u-u_h\|_{H^1}^2+\|\hat{u}-\hat{u_h}\|_{H^1}^2 \leq (1+\gamma)^2h^2\left[C(\Omega)\|D^2u\|_{L^2(\Omega)}^2+C(\Gamma)\|D^2\hat{u}\|_{L^2(\Gamma)}^2\right]$$

Taking the square root of both sides we obtain a bound on the H^1-norm of the approximation error $e\vec{u} = (u,\hat{u})-(u_h,\hat{u}_h)$

$$e_{tot} = \sqrt{\|u-u_h\|_{H^1}^2+\|\hat{u}-\hat{u_h}\|_{H^1}^2} \leq (1+\gamma)h\sqrt{C(\Omega)\|D^2u\|_{L^2(\Omega)}^2+C(\Gamma)\|D^2\hat{u}\|_{L^2(\Gamma)}^2}. \tag{28}$$

Calculating e_{tot} for five different mesh refinements, approximately halving h for each refinement we should, from the estimate above expect h^1-convergence - for H^2 regular solutions. We use the manufactured solutions given last in table 1, $\gamma = 100$ and compute e_{tot} for four successive refinements on h. Additionally, [Braess, 2007] p. 79 shows that under certain circumstances[2] the following bound holds for $P1, P2, Q1, Q2$[3] type elements

$$\|u-u_h\|_{H^m} \leq Ch^{t-m}\|u\|_{H^t} \tag{29}$$

for interpolation using $t-1$ order polynomials. This means we should expect h^2 convergence for H^3 regular solutions and h^t convergence when measuring the error in the L^2-norm

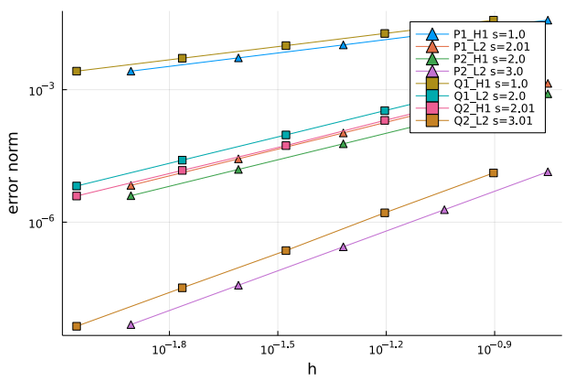

Figure 3: Log-log plot of error measured in both the L^2 -norm and the H^1-norm of the boundary problem (23), (24) on the domain (figure 2.) using manufactured solutions given last in table 1.

Figure 3. shows that we obtain the expected convergence rates for both triangular and quadrilateral elements. From (28) we see that the error also depends on the coupling factor γ and we should expect an increase in the error if γ increases.

We will not explain the shape of the curves in figure 4. but we note that the error associated with an increase in γ is minuscule as $\Delta e = 6.0 \cdot 10^{-5}$ using $P1$ type elements while $\Delta\gamma = 1000$. With this result we will not further investigate how the coupling factor changes the accuracy of our approximation and we simply set $\gamma = 1$ in the rest of this chapter.

[2]Maybe say something about these requirement, and if they are applicable to our problem?
[3]$Q2 = 9$ node quadrilateral element.

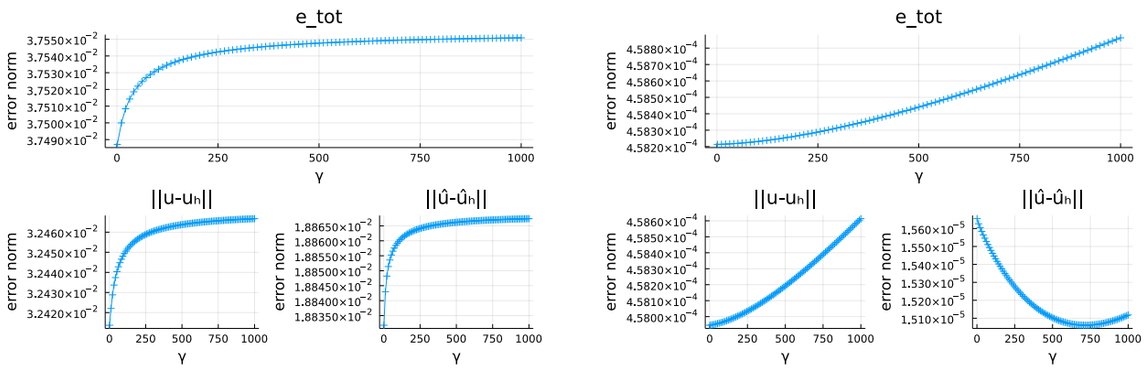

(a) Order 1 triangular elements

(b) Order 2 triangular elements

Figure 4: Error as a function of the coupling factor γ.

From Appendix A, and Lax Milgrams theorem we know that our variational form (27) admits solution $(u, \hat{u}) \in H^1 \notin H^2$, however from estimate (28) we see that that the regularity of the solution clearly effects the bound on the error. To study convergence for these types of solutions we consider a manufactured solution $u_m = \sin|y|$ or equivalently

$$\begin{cases} u_1 &= \sin(y) \text{ on } \Omega_1 \\ u_2 &= -\sin(y) \text{ on } \Omega_2 \\ \hat{u} &= 0 \text{ on } \Gamma. \end{cases} \tag{30}$$

Where, for simplicity, we have set $\hat{u}_m = 0$ as the solution on the curve Γ, We have

$$u(x,y) = \sin|y|, \qquad \frac{d}{dy}u(x,y) = \frac{y}{|y|}\cos|y| = \text{sgn}(y)\cos|y|$$
$$\frac{d^2}{dy^2}u(x,y) = \frac{d}{dy}\text{sgn}(y)\cos|y| + \text{sgn}(y)\frac{d}{dy}\cos|x|$$

since $\cos(y)$ is symmetric we have $\cos|y| = \cos(y)$ and we can rewrite $\text{sgn}(y) = 2H(y) - 1$ where $H(y)$ is the Heaviside function with the known distributional derivative $\delta(y)$, namely the Dirac-delta function. Whence, we get

$$\frac{d^2}{dy^2}u(x,y) = 2\delta(y) - \text{sgn}(y)\sin(y)$$

where we have simplified $2\delta(y)\cos(y) = 2\delta(y)$ since $\cos(y) = 1$ in $y = 0$ and $\delta(y) = 0$ when $y \neq 0$. The corresponding source terms to our manufactured solutions are

$$f_1 = -\sin(y), \qquad f_2 = \sin(y)$$
$$\hat{f} = 0, \qquad g = -2\sin(y) - \gamma\sin(y).$$

Now, considering the regularity of $u(x,y) = u(y)$ on Ω we want to show - for $H^1(\Omega)$ regularity, that u has a weak derivative Du and that $\|Du\|_{L^2(\Omega)} < \infty$. We need to find a measurable function $Du : \Omega \to \mathbb{R}$ such that

$$\int_\Omega u(y)\phi'(y) = -\int_\Omega Du(y)\phi(y)$$

$\forall$ smooth functions $\phi : \Omega \to \mathbb{R}$ with compact support in Ω. Using integration by parts we have

$$\int_\Omega \sin|y|\phi'(y) = \int_{\Omega_1} \sin(y) - \int_{\Omega_2} \sin(y) = \big[\sin(y)\phi(y)\big]_{\Omega_1} - \int_{\Omega_1} \cos(y)\phi(y) - \big[\sin(y)\phi(y)\big]_{\Omega_2} + \int_{\Omega_2} \cos(y)\phi(y)$$

Since ϕ has compact support and $\sin(0) = 0$ we get

$$\int_\Omega \sin|y|\phi'(y) = -\int_{\Omega_1} \cos(y)\phi(y) + \int_{\Omega_2} \cos(y)\phi(y) = -\int_\Omega \text{sgn}(y)\cos(y)\phi(y)$$

And thus $Du(y) = \text{sgn}(y)\cos(y) = \nabla u(y)$.
Next, we have

$$\|Du\|^2_{L^2(\Omega} = \int_\Omega |\text{sgn}(y)\cos(y)| = \int_\Omega |\cos(y)| < \infty$$

Which concludes $u \in H^1(\Omega)$.
Considering the second derivative of u on the two subdomains Ω_1, Ω_2 we have

$$u''(y) = \begin{cases} -\sin(y) & \text{on } \Omega_1 \\ \sin(y) & \text{on } \Omega_2 \end{cases}$$

Which we know have to agree with the weak derivative on the domains. Again, using integration by parts we obtain

$$\begin{aligned} \int_\Omega u'\phi' &= \int_{\Omega_1} \cos(y)\phi'(y) - \int_{\Omega_2} \cos(y)\phi'(y) = \big[\cos(y)\phi(y)\big]_{\Omega_1} + \int_{\Omega_1} \sin(y)\phi(y) - \big[\cos(y)\phi(y)\big]_{\Omega_2} - \int_{\Omega_2} \sin(y)\phi(y) \\ &= (0 - \phi(0)) - (\phi(0) - 0) + \int_\Omega \text{sgn}(y)\sin(y)\phi(y) \\ &= -2\phi(0) + \int_\Omega \text{sgn}(y)\sin(y)\phi(y) \quad \underbrace{\overset{!}{=}}_{\text{should equal}} \quad -\int_\Omega u''(y)\phi(y) = \int_\Omega \text{sgn}(y)\sin(y)\phi(y) \end{aligned}$$

which should hold for all $\phi \in C_c^\infty(\Omega)$ but only holds when $\phi(0) = 0$. Therefore D^2u does not exist and $u \notin H^2(\Omega)$. We do, however, note that the disagreement lies on Γ and that we do have $u \in H^2(\Omega_1 \cup \Omega_2)$.

Recalling estimate (28)

$$e_{tot} = \sqrt{\|u - u_h\|_{H^1}^2 + \|\hat{u} - \hat{u_h}\|_{H^1}^2} \leq (1+\gamma)h\sqrt{C(\Omega)\|D^2u\|_{L^2(\Omega)}^2 + C(\Gamma)\|D^2\hat{u}\|_{L^2(\Gamma)}^2}.$$

we see that without a bound on $\|D^2\hat{u}\|$ we cannot guarantee first order convergence of e_{tot} when refining the mesh parameter h.

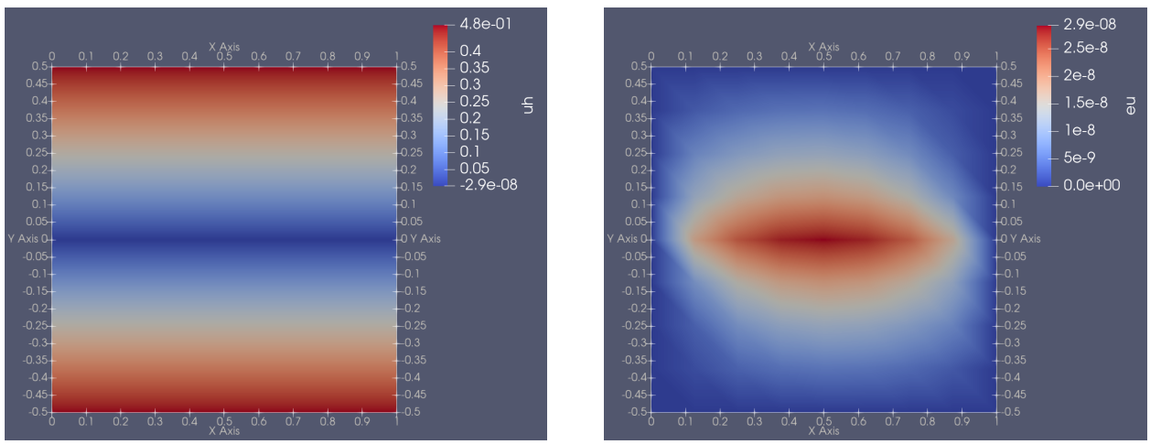

(a) Computed solution

(b) Error

Figure 5: Computed solution and corresponding error for boundary problem (23), (24) with manufactured solutions (30).

The figures above shows the computed solution u_h over the domain $\Omega = \Omega_1 \cup \Omega_2$ and the corresponding error $eu = u - u_h$ for $h \approx 0.17$. We see that the highest error is located on and around Γ . From figure (a), the computed solution u_h on Γ is $-2.9 \cdot 10^{-8}$, while we know that the true solution $u = 0$ on Γ which amounts for the error in (b).
Figure 6. shows that the convergence is almost not effected by the lower regularity on u. The calculated slope is 0.994 while with H^2 regularity on the whole of the domain Ω we should expect 1.0. With higher refinement of h or by considering a part of the domain closer to the error in fig.1 (b) we should expect a further decrease in convergence rate.

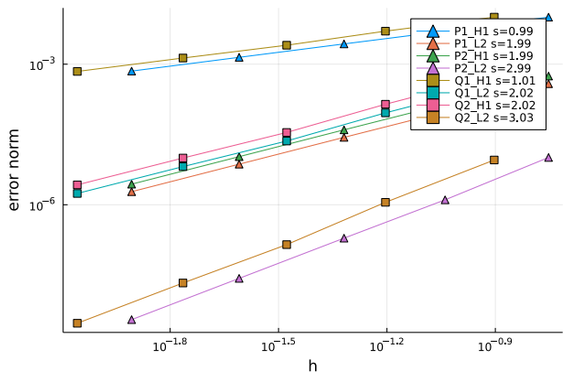

Figure 6: Log-log plot of error measured in both the L^2 -norm and the H^1-norm of the boundary problem (21), (22) on the domain (figure 2.) using manufactured solutions (25).

5.1.2 Nonconvex subdomain

We want to consider the variational problem (27) on the square domain $\Omega = \Omega_1 \cup \Omega_2$ with vertices $(-1,1),(1,1),(1,-1)$ and $(-1,-1)$. We define $\Omega_2 = \{(x,y) \in \Omega : (x,y) < 0\}$, $\Omega_1 = \{(x,y) \in \Omega : (x,y) \notin \Omega_2\}$ and $\Gamma = \{(x,y) \in \Omega : (x,y) \in \Omega_1 \cap \Omega_2\}$. The reason we want to consider a

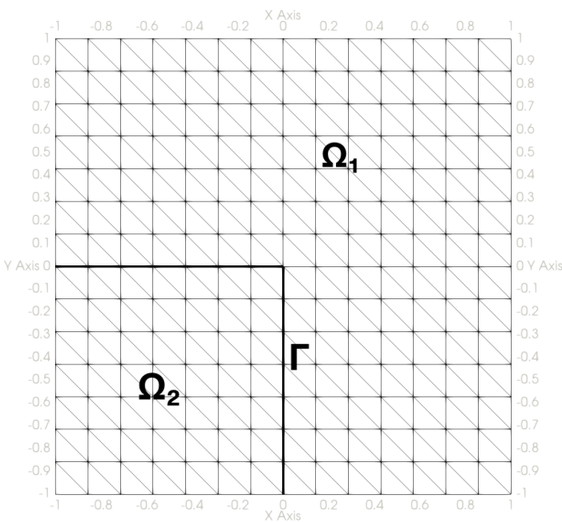

Figure 7: Meshed 2D/1D domain

nonconvex domain Ω_1 is that convexity is a well known requirement on elliptic problems to ensure H^2 regularity of the solution u, see e.g. [Grisvard, 2011]. We note that the corresponding strong formulation of the variational problem (27) equal (23), (24) but with different definitions on the unit vectors ν_1 and ν_2, this will be emphasised later. We follow our standard procedure constructing manufactured solutions, but we must pay extra attention to how we implement the solution in Γ. Since $\Gamma = \Gamma_1 \cup \Gamma_2$ where $\Gamma_1 = \{(x,y) \in \Gamma : y = 0\}$ and $\Gamma_2 = \{(x,y) \in \Gamma : x = 0\}$ we will implement the manufactured solution $\hat{u}_m = \hat{u}$ as

$$\hat{u}(x,y) = \hat{u}|_{\Gamma_1} + \hat{u}|_{\Gamma_2}$$

Recall that we require $\hat{u}(x,y) \in H^1(\Omega)$ and furthermore $\vec{u} = (u,\hat{u}) \in H^2(\Omega) \times H^2(\Gamma)$ to guarantee first order convergence. For simplicity we consider $\hat{u}|_{\Gamma_1}$ and $\hat{u}|_{\Gamma_2}$ are $C^k(\Gamma)$ with $k \geq 2$. Integration by parts then gives us

$$\begin{aligned}\int_\Gamma \nabla\hat{u}\phi' &= \int_{\Gamma_1} \partial_x\hat{u}\phi' + \int_{\Gamma_2} \partial_y\hat{u}\phi' = [\partial_x\hat{u}\phi]_{\partial\Gamma_1} + [\partial_y\hat{u}\phi]_{\partial\Gamma_2} - \int_{\Gamma_1} \partial_{xx}\hat{u}\phi - \int_{\Gamma_2} \partial_{yy}\hat{u}\phi \\ &= [(\partial_x\hat{u}(x,y) - \partial_y\hat{u}(x,y))\phi(x,y)]_{(0,0)} - \int_\Gamma \Delta\hat{u}\phi\end{aligned}$$

As in 5.1.1, $D^2\hat{u} \overset{!}{=} \Delta\hat{u}$ to obtain $\hat{u} \in H^2(\Gamma)$, therefore we require continuity in $(0,0)$ i.e. $\partial_x\hat{u}(0,0) = \partial_y\hat{u}(0,0)$ or equivalently $\nabla\hat{u} \in C^0(\Gamma)$ to ensure $\hat{u} \in H^2(\Gamma)$. Experiments show that with the above

satisfied and thus $u, \hat{u} \in H^2$ we get the expected convergence rates for manufactured solutions $(u_m, \hat{u}_m) \in H^2(\Omega) \times H^2(\Gamma)$.

One reason that higher regularity of the solution to a boundary value problem and convexity of the domain often imply each other is that nonconvex domains, like Ω_1 and a particular boundary value problem can have underlying singularities. [Elman et al., 2014] investigates the solution to the Poisson boundary value problem $-\Delta u = 1$ on a domain similar to Ω_1 with boundary conditions $u = 0$ on $\partial\Omega_1$. They show that the solution u_h can be closely approximated at the origin by

$$u = r^{2/3}\sin((2\theta + \pi)/3) \tag{31}$$

Where r represents the radial distance to the center of figure 1. and θ the the angel with the vertical axis. We note that the radial derivatives of u are unbounded at the origin. Setting

$$u_1(r, \theta) = r^{2/3}\sin((2\theta + \pi)/3) \quad \text{on} \quad \Omega_1 \tag{32}$$

$$u_2 = 0 \quad \text{on} \quad \Omega_2 \tag{33}$$

$$\hat{u} = 0 \quad \text{on} \quad \Gamma \tag{34}$$

we can create a similar scenario as the Poisson boundary value problem on a nonconvex domain. We use the definitions

$$r(x, y) := \sqrt{x^2 + y^2} \tag{35}$$

$$\theta(x, y) := \begin{cases} \cos^{-1}(\frac{x}{r}) & y \geq 0 \\ -\cos^{-1}(\frac{x}{r}) & y < 0 \end{cases} \tag{36}$$

and note that $\theta(0, y < 0) = -\frac{\pi}{2} \to u_1 = 0$ and $\theta(x < 0, 0) = -1 \to u_1 = 0$ such that the continuity condition $u_1 - u_2 = 0$ on Γ is fulfilled. The Robin condition given last in (24) is fulfilled by defining ν_1 as the piecewise unit normal vector (in polar coordinates) from Ω_1 over Γ_1 and Γ_2, ν_2 is defined similarly, but opposite (over Ω_2).

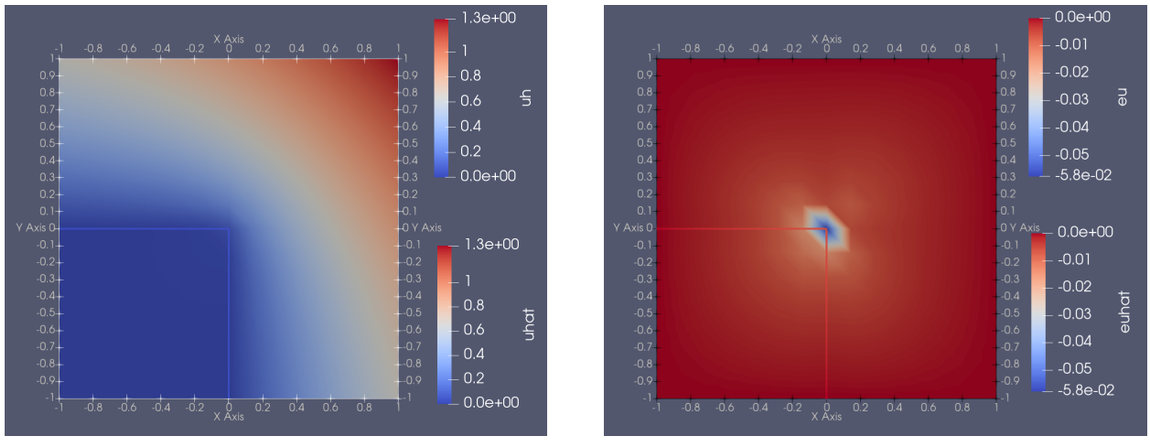

(a) Computed solution

(b) Error

Figure 8: Computed solution and corresponding error for boundary problem (23), (24) with manufactured solutions (32)-(35).

From figure 8. (a) we see that the computed solution cannot approximate the singularity at the origin, this amounts for the error in figure 8. (b). Since $u \in H^1(\Omega) \notin H^2(\Omega)$ we cannot bound the error by (28). However, [Elman et al., 2014] establishes, for the Poisson boundary value problem on the L-shaped domain, the bound

$$\|\nabla(u - u_h)\|_{L^2(\Omega)} \leq C_m h^{\frac{2}{3}-\epsilon} \tag{37}$$

Where m is the order of interpolating polynomials and $\epsilon > 0$ is an arbitrary constant. Figure 10. shows that the bound (38) holds for four successive refinements on h and for $P1, P2, Q1, Q2$ type elements.

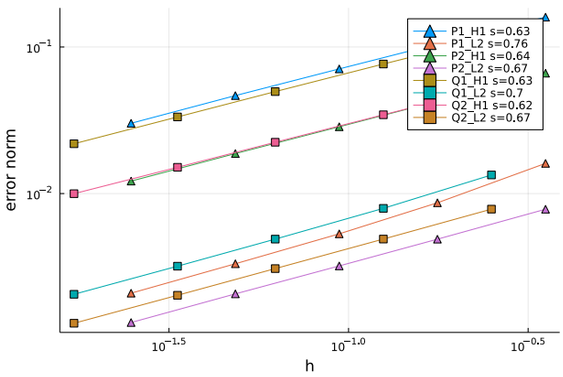

Figure 9: Log-log plot of error against mesh refinement.

5.1.3 Unstructured mesh

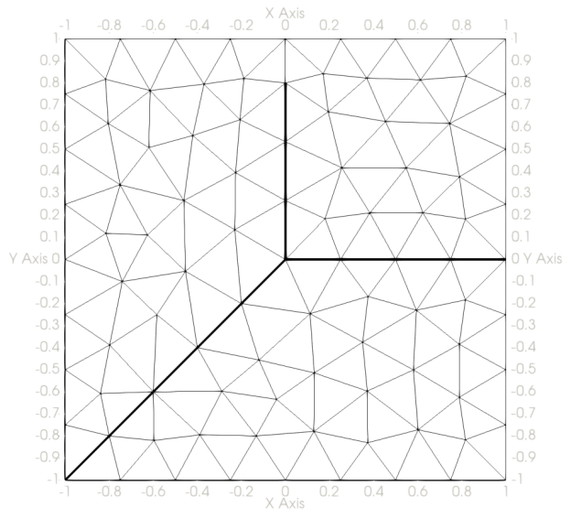

Figure 10: Embedded 1D domain Γ in 2D domain Ω.

Previously we have only considered structured meshes, which we have shown provide regular and uniform errors (Figure 5) excluding the point of singularity in (Figure 8). However, considering a more irregular 1D domain Γ, we are forced to use a less structured mesh to be able to embed $\Gamma \subset \Omega$. Recalling estimate (28) we know that the bound on the error is dependent on the length between the nodes h. Considering only our 2D domain, consisting of triangle elements Δ_k we should expect a different error bound depending on the length of the longest triangle edge h_k. Indeed, following [Elman et al., 2014] p. 39 we can establish the bound

$$\|D(u - u_h)^2_{\Delta_k}\| \leq 2\frac{h_k^2}{|\Delta_k|}\|D(\bar{u} - \bar{u}_h)\|^2_{\Delta_*}. \tag{38}$$

$\bar{u}$ denotes the mapped function on a reference element Δ_*. (39) shows that a large aspect ratio $\frac{h_k^2}{|\Delta_k|}$, i.e. long triangle edges w.r.t the area of the triangle correspond to a high bound on the element error, with the lowest bound obtained with equilateral elements Δ_k.
We consider the 2D/1D domain given in figure 10 and manufactured solutions

$$u_m = x^3 - y^3 \qquad \text{on} \qquad \Omega \tag{39}$$

$$\hat{u}_m = x^3 + y^3 \qquad \text{on} \qquad \Gamma. \tag{40}$$

Since $u_m \in C^2(\Omega)$, the strong formulation of (21) is simplified to

$$\begin{aligned} -\Delta u &= f \qquad \text{on} \qquad \Omega \\ u &= u_m \qquad \text{on} \quad \partial\Omega \setminus \Gamma \end{aligned} \tag{41}$$

$$\text{on } \Gamma \quad \begin{cases} -\Delta\hat{u} + \gamma(\hat{u} - u) & = \hat{f} \\ \hat{u}|_{\partial\Gamma} & = \hat{u}_m \\ 0 & = \gamma(u - \hat{u}) + g \end{cases} . \tag{42}$$

Using order $P1, P2$[4] type elements we will experience an interpolation error in our solution $u_h, \hat{u}_h$ but we want to ensure convergence with the more complex Γ and as a consequence, the more irregular mesh. We enforce our manufactured solutions by setting the source terms

$$f = -\Delta u \tag{43}$$
$$g = -\gamma(u - \hat{u}) \tag{44}$$

and to enforce $\hat{u}_m$ on Γ we divide Γ into

$$\Gamma_{xy} = \begin{cases} \Gamma & x, y \in (-1, 0) \\ \emptyset & \text{else} \end{cases} \quad \Gamma_x = \begin{cases} \Gamma & x \in (0, 1), y = 0 \\ \emptyset & \text{else} \end{cases}$$
$$\Gamma_y = \begin{cases} \Gamma & y \in (0, 1), x = 0 \\ \emptyset & \text{else} \end{cases}$$

Now, we can separate the different gradients given as

$$\nabla_{\Gamma_{xy}} = \frac{1}{\sqrt{2}} \left(\frac{\partial}{\partial x}, \frac{\partial}{\partial x} \right), \qquad \nabla_{\Gamma_x} = \frac{\partial}{\partial x}, \qquad \nabla_{\Gamma_y} = \frac{\partial}{\partial y}$$

and calculate the different source terms

$$\hat{f}_1 = -\nabla_{\Gamma_{xy}} \cdot \nabla_{\Gamma_{xy}} u = \frac{1}{2} \left(\frac{\partial^2 \hat{u}_m}{\partial x^2} + \frac{\partial^2 \hat{u}_m}{\partial y^2} \right), \qquad \hat{f}_2 = \nabla_{\Gamma_x} \cdot \nabla_{\Gamma_x} = \frac{\partial^2 \hat{u}_m}{\partial x^2}$$
$$\hat{f}_3 = \nabla_{\Gamma_y} \cdot \nabla_{\Gamma_y} = \frac{\partial^2 \hat{u}_m}{\partial y^2}$$

Notice that the $\nabla_{\Gamma_{xy}} \hat{u} = \nabla_{\Gamma_x} \hat{u} = \nabla_{\Gamma_y} \hat{u}$ at the branch point $(0, 0)$ so $\hat{u} \in C^1(\Gamma)$ and thus from our reasoning in the nonconvex domain, $\hat{u} \in H^2(\Gamma)$ Figure 11. (a) shows that on a unstructured grid

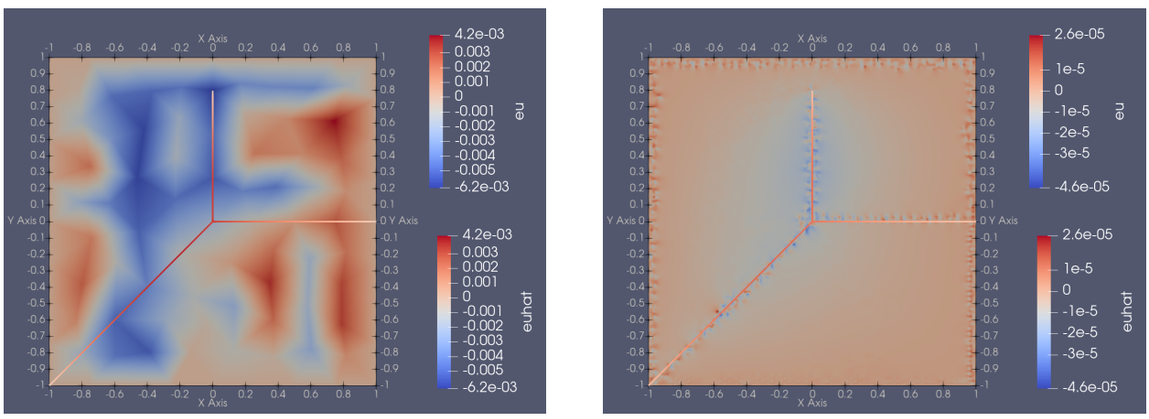

(a) Error on coarsest mesh.

(b) Error in finest mesh.

Figure 11: Error $u - u_h$ of the boundary problem with manufactured solutions (42), (43) with mesh refinement $h_k \approx 0.35 \to 0.02$.

the location of the interpolation error is decided by the aspect ratio of the triangle elements. The nodes shared between triangle elements with high aspect ratio will exhibit the highest error. Mesh refinement, figure (b) allows for more equilateral triangle elements but retains the more "bad" elements along the boundary $\partial\Omega$ and Γ. The domain Γ is partitioned into equal distance nodes, therefore the error on Γ is more regular and the error is concentrated away from the boundary points $\partial\Gamma$ where we enforce $\hat{u}_h = \hat{u}_m$ as Dirichlet boundary conditions.

[4]This curve Γ does not allow for discretation using Qk type elements. Gmsh allows for combined element types, but this functionality is not yet implemented in Gridap, and will thus not be investigated.

Estimate (39) is dependent on the minimum angle condition (definition ..), i.e. we must prevent that $|\Delta_k| \to 0$ as we refine the mesh. Gmsh [Geuzaine and Remacle, 2009] does this automatically and is done by refining the mesh by scaling the mesh size elements and then remeshing the surface $\Omega \cup \Gamma$. To measure the aspect ratio of the computed triangle elements, Gmsh [Geuzaine and Remacle, 2009] uses a metric defined by

$$\eta = 2R_1/R_2$$

Where $R_1 =$ inscribed radius, $R_2 =$ circumscribed radius. By the relations

$$R_2 = \frac{abc}{4R_1 s}$$
$$R_1 = \sqrt{\frac{(s-a)(s-b)(s-c)}{s}}$$

where a, b, c are the triangle edges and $s = \frac{1}{2}(a+b+c)$ is the semiperimeter. By the formula

$$|\Delta_k| = \sqrt{s(s-a)(s-b)(s-c)}$$

which is often denotes as Heron's formula. We then have

$$\eta = \frac{2R_1 \cdot 4R_1 s}{abc} = \frac{8R_1^2 s}{abc} = \frac{8|\Delta_k|^2}{sabc} = \frac{16|\Delta_k|^2}{a^2bc + b^2ac + c^2ab}$$

Choosing a, b or c as our longest triangle edge h_k we see that increasing $\frac{h_k^2}{|\Delta_k|}$ i.e. minimizing the triangle area or increasing h_k has the effect of lowering η. We also note that for an equilateral triangle we have the best possible aspect ratio and $\eta = 1$. Table 2. shows that the aspect ratio does

scale	element id	h_{max}	η
1.0	71	0.3504	0.767
0.5	97	0.1572	0.823
0.25	395	0.0773	0.686
0.125	628	0.0437	0.787
0.0625	1158	0.02136	0.737

Table 2: Worst elements according to η and corresponding max edge length for five different scaling factors.

not increase (η decrease) as we refine the mesh and that h_{max} is approximately halved for each scaling factor.

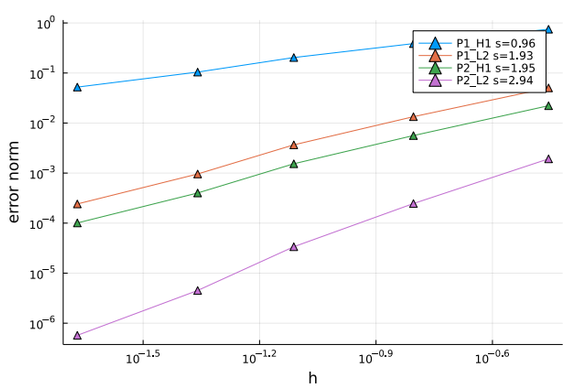

Figure 12: Log-log plot of error against mesh refinement.

Figure 12. shows that we obtain close to expected converge rate, but the more varying quality of the triangle elements slows down the convergence.